Search for quarks using a flash tube chamber

1971 J. Phys. A: Gen. Phys. 4 895

(http://iopscience.iop.org/0022-3689/4/6/016)

J. Phys. A: Gen. Phys., 1971, Vol. 4. Printed in Great Britain

Search for quarks using a flash tube chamber

F. ASHTON, R. B. COATS, J. KING, K. TSUJI† and A. W. WOLFENDALE

Physics Department, University of Durham, Durham, England

MS. received 1*st April* 1971, *in revised form* 28*th April* 1971

Abstract. A large flash tube chamber has been constructed with the object of searching for relativistic $e/3$ quarks in extensive air showers (EAS) at ground level. Experiments have been carried out to examine the applicability of the method; in particular, the response of the apparatus to muons of varying ionization has been investigated. It has been found that the logarithmic increase in ionization loss is reflected accurately in the variation of mean flash-tube efficiency with muon energy, which gives confidence in the method. Furthermore, the fluctuation in number of flashed tubes along a muon track is close to expectation. In a preliminary search no $e/3$ quarks have been detected amongst 439 carefully measured penetrating EAS particles, and already there is an inconsistency with the data of McCusker and Cairns.

1. Introduction

A systematic search for quarks in cosmic rays has been conducted at Durham since 1966. The experiments already completed are:

(i) A search for relativistic $e/3$ and $2e/3$ quarks using a scintillation-counter telescope.

(ii) A search for heavy mass, low velocity particles, irrespective of their charge.

(iii) A search for relativistic $4e/3$, $5e/3$ and $7e/3$ particles.

All these experiments gave negative results and the intensity limits obtained are shown in table 1. However, it should be noted that because of the nature of the electronic selection systems used, the limits refer to quarks arriving at sea level with an accompaniment of about 1 particle/m^2 or less.

Table 1. Intensity limits of unaccompanied† quarks at sea level, as observed at Durham

Experiment number	Charge state investigated	Upper limit to quark intensity	Reference
1	$e/3$	$1{\cdot}2\times10^{-10}$ cm^{-2} s^{-1} sr^{-1}	Ashton *et al.* (1968)
	$2e/3$	$8{\cdot}0\times10^{-11}$ cm^{-2} s^{-1} sr^{-1}	
2	Heavy mass irrespective of charge	$4{\cdot}9\times10^{-10}$ cm^{-2} s^{-1} sr^{-1} for β in the region of $0{\cdot}8c$	Ashton *et al.* (1969)
3	$4e/3$, $5e/3$ and $7e/3$	$8{\cdot}2\times10^{-10}$ cm^{-2} s^{-1} sr^{-1}	Ashton and King (1971)

† Less than about 1 particle/m^2.

In 1969 attention was turned to a search for quarks in extensive air showers as a result of the work of McCusker and Cairns (1969) and Cairns *et al.* (1969) who

† On leave from Kinki University, Japan.

presented evidence for the existence of particles of charge $2e/3$. The evidence produced to date, however, is not entirely clear cut and has been criticized by a number of workers (eg Adair and Kasha 1969, Kiraly and Wolfendale 1970, Hazen 1971). A fact of relevance to the present search is the remark by Kiraly and Wolfendale that if the Sydney group have detected quarks at all then they are more likely to be of the $e/3$ variety. Based on this, the present search is directed towards $e/3$ rather than $2e/3$ particles.

To check the results of Cairns *et al.*, a visual detector of large aperture is required in which ionization measurements can be made on individual tracks in extensive air showers. The neon flash-tube, like many other detectors, relies for its operation on the ionization left by a charged particle and in view of the fact that its sensitivity to the ionization can be varied at will, for example by varying the time delay between the instant of traversal and the application of the high voltage pulse, it is in principle a quark detector. Large arrays of flash-tubes can be operated with ease and there is thus the possibility of making a useful search for quarks with an alternative technique to the more usual cloud chamber method. Accordingly a large neon flash tube chamber (of sensitive volume 3·04 m high × 1·51 m wide × 1·08 m deep) has been constructed with which to continue the search.

We regard the following to be of paramount importance in quark searches:

(i) A demonstration that the detector is sensitive to ionization and a firm estimate of the response expected for fractionally charged particles.

(ii) A measurement of the distribution of response for single muons (preferably as a function of their momentum) from which the probability of such a particle simulating a quark may be estimated.

The present work endeavours to demonstrate that the flash tube chamber satisfies these requirements and it gives the result of a preliminary search for $e/3$ quarks in extensive air showers.

2. Apparatus

A scale diagram of the flash tube chamber is shown in figure 1. The chamber itself is situated in an enclosure of rectangular cross section made of 30 cm thick barytes concrete walls, the roof being 15 cm of lead mounted on 1·3 cm thick steel plates. This shielding is designed to absorb the electronic component of extensive air showers but allow muons, quarks etc to penetrate it and be observed in the chamber (one,

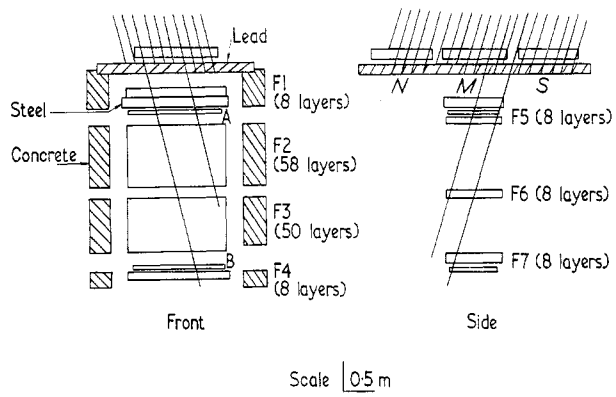

Figure 1. Scale diagram of the prototype flash-tube chamber.

at least, of the Sydney 'quarks' had penetrated 15 cm lead and we assume implicitly that the majority of EAS quarks, assuming that they exist, are able to penetrate the lead—a not unreasonable assumption if they have penetrated the majority of the atmosphere already). Air showers are selected by a coincidence between the three liquid scintillators N, M and S situated above the lead. The scintillators are each of area 1·24 m^2.

Single muons can also be selected by a twofold coincidence between the plastic scintillators A and B.

The chamber itself uses flash tubes of mean internal diameter 1·58 cm and external diameter 1·78 cm, the gas filling being neon to a pressure of 60 cm mercury. The tubes are stacked side by side and electrodes are situated 3·3 cm apart thus enclosing two layers. The front view contains four blocks of tubes: F1 (8 layers), F2 (58 layers), F3 (50 layers) and F4 (8 layers). The side view contains three blocks of tubes: F5 (8 layers), F6 (8 layers) and F7 (8 layers) (these tubes were only operated for a small fraction of the running time). In all, the chamber uses 11 670 tubes. The 15·2 cm thick steel absorber situated below F1 is for assisting in recognizing penetrating particles and also for indicating neutral nuclear active particles.

3. Flash tube characteristics

The most important characteristic for the present application is the efficiency–time delay variation, by the term 'internal efficiency' being meant the average probability of a tube flashing when a particle traverses the gas (to be even more specific it refers to the probability of a flash being recorded photographically). Figure 2 shows this variation for single muons selected by the twofold coincidence system.

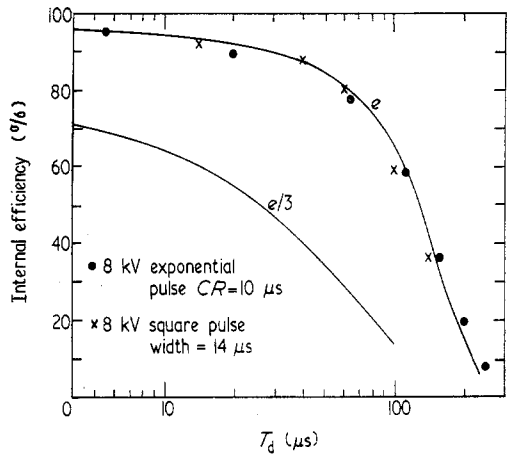

Figure 2. The variation of internal efficiency with time delay. The best fit curve through the experimental points has $af_1Q = 12$ and accordingly that for $e/3$ quarks (of the same mean Lorentz factor) has $af_1Q = 1{\cdot}33$.

Measurements are shown for exponential and square pulses applied to the chamber electrodes, the exponential pulse had a peak height of 8 kV and $CR = 10\ \mu s$ while the square pulse had a peak height of 8 kV and a full width at half height of 14 μs. The decrease of efficiency with time delay T_D arises from the loss of the initial electrons by diffusion to the glass walls of the tube in the time interval between the passage of the particle and the application of the high voltage pulse to the chamber.

The process of electron diffusion in the flash tube has been studied empirically by Coxell and Wolfendale (1960) and the detailed theory has been given by Lloyd (1960).

Lloyd gives universal curves for the expected variation of efficiency with time delay in terms of the parameter af_1Q where a is the tube radius, f_1 is the average probability that a single electron is capable of producing a flash when the high voltage pulse is applied, and Q is the average number of initial electrons produced per unit length in the neon gas. A curve with $af_1Q = 12$ is found to give the best fit to the measurements for single muons and this is designated e in figure 2. Q can be estimated from a knowledge of the average rate of energy loss and the energy per ion pair, and thus f_1 can be found. For muons of energy 2·1 GeV, the estimated median value for the calibration run, Sternheimer (1956) gives a rate of energy loss of 1·8 MeV g^{-1} cm^2 in neon, and using an energy loss per ion pair of 37·6 eV (Jesse and Sadauskis 1955) $Q = 38$ ion pairs/cm. In fact, the relevant number in the present case will be nearer 30 because of the contribution to the mean energy loss of rare energetic encounters in which the struck electron has an energy greater than that required to traverse the gas (and thus does not give its full contribution to the detected ionization). With $Q = 30$, and $a = 0{\cdot}79$ cm, $f_1 = 0{\cdot}5$. This value is regarded as reasonable (and agrees with Lloyd's value from an experimental comparison).

The fact that the shape of the efficiency–time delay curve is correct can be regarded as a measure of proof that the efficiency depends in a straightforward way on the number of electrons left in the tube at the time the pulse is applied. Essentially, it means that f_1 is independent of the number of electrons present, so that the theory should be applicable to a quark as it is to a muon provided that Q is multiplied by the square of the quark charge (in units of electron charge squared). The expected efficiency–time delay curve for $e/3$ quarks with the same Lorentz factor as the calibration muons is thus given by the Lloyd curve with $af_1Q = (1/9) \times 12 = 1{\cdot}33$. The result is shown in figure 2, designated $e/3$.

Confirmation of the assertion that the efficiency is related to particle ionization in a known way is given later in § 5.

A further characteristic of importance is the variation of efficiency with the magnitude of the electric field which is applied to the flash tubes. The result for $T_D = 40\ \mu s$ is shown in figure 3.

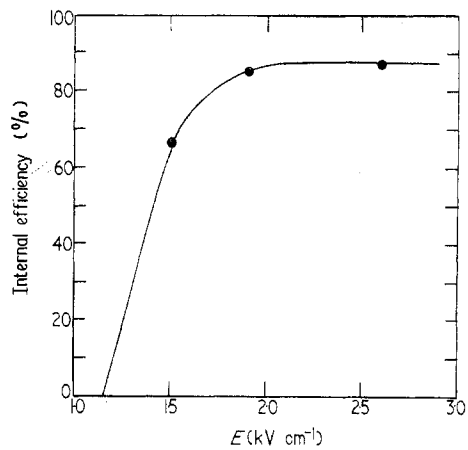

Figure 3. The variation of internal efficiency with electric field, E. The measurements are for a square pulse of width 14 μs and $T_D = 40\ \mu s$. The electrode separation is 3·3 cm.

It is apparent from figure 2 that the difference between the efficiency for e and $e/3$ particles increases as T_D increases and hence the probability of spurious identification falls as T_D is made bigger. However, a limit is set when an $e/3$ track has so few flashes that it merges into the background of stray flashes, these flashes being more numerous when EAS triggering is adopted because of the accompanying γ rays. In the work to be described measurements have been made at $T_D = 20\ \mu s$ and $T_D = 40\ \mu s$, the latter time delay being close to the optimum when the background problem is also considered.

4. Air shower data

Air showers have been selected by a coincidence between the three liquid scintillators, N, M and S shown in figure 1. For all the running time the discrimination level on each scintillator was set so as to accept a minimum of about 50 particles through it and the average rate of coincidences was $3{\cdot}6\ h^{-1}$. A wide range of shower sizes could trigger the selection system, varying from small showers whose axes fell close to the chamber to large showers whose axes fell a long distance away. Using accepted values of the number spectrum and lateral distribution of electrons at sea level the median shower size is calculated to be of the order of 2×10^6 particles and the median core distance of showers is about 30 m.

So far the chamber has been operated for 162 h using a high voltage exponential pulse of peak height 8 kV and $CR = 10\ \mu s$ with $T_D = 20\ \mu s$ (run 1 data), for 250 h with an almost square high voltage pulse of peak height 8 kV and full width at half height of 14 μs (run 2 data), and for 254 h with the same pulse as for run 2 but with a somewhat different electrode geometry (run 3 data—details of the run 3 geometry are given later). The time delay for runs 2 and 3 was 40 μs. The yield of measurable events obtained and other parameters are shown in tables 2 and 3.

Table 2. Basic experimental data

	Run 1 $T_D = 20\ \mu s$	Run 2 $T_D = 40\ \mu s$	Run 3 $T_D = 40\ \mu s$
Running time	162 h	250 h	254 h
Total number of triggers	760	900	748
Total number of measurable triggers	79	129	79
Percentage of triggers that gave at least one measurable track	10%	14%	11%
Total number of measured tracks	111	213	115

A measurable track is one in which the particle traverses F1, F2, F3 and F4 (figure 1) and is accompanied by at least one parallel track in F2 or F3 of length greater than 90 cm.

In the analysis a stringent requirement was adopted that a track should be accepted for measurement only if it corresponded to a particle which had traversed the whole of F1, F2, F3, F4 (figure 1) and which was accompanied by at least one parallel track of length greater than 90 cm in F2 or F3. To be accepted as parallel, tracks had to be within $\pm 2{\cdot}5\ ^\circ$ of one another in the front view. The number of flashes N_f (in F2 + F3) along the estimated trajectory of each accepted track was counted and the mean projected zenith angle θ of the shower (in the front plane) was noted.

Table 3. The frequency distribution of the number of triggers N having n measurable tracks

Number of measurable tracks n per event	Run 1 $T_D = 20\ \mu s$ N	Run 1 $N \times n$	Run 2 $T_D = 40\ \mu s$ N	Run 2 $N \times n$	Run 3 $T_D = 40\ \mu s$ N	Run 3 $N \times n$
1	54	54	75	75	54	54
2	18	36	35	70	19	38
3	7	21	12	36	3	9
4	0	0	4	16	1	4
5	0	0	2	10	2	10
6	0	0	1	6	0	0
Sum	79	111	129	213	79	115

Many of the photographs show weak showers with penetrating particles travelling obliquely and not satisfying the criteria. Only a few show very dense showers that render the identification of in-geometry penetrating particles impossible. The frequency distributions are given in figures 4 and 5 for both muon calibration and air

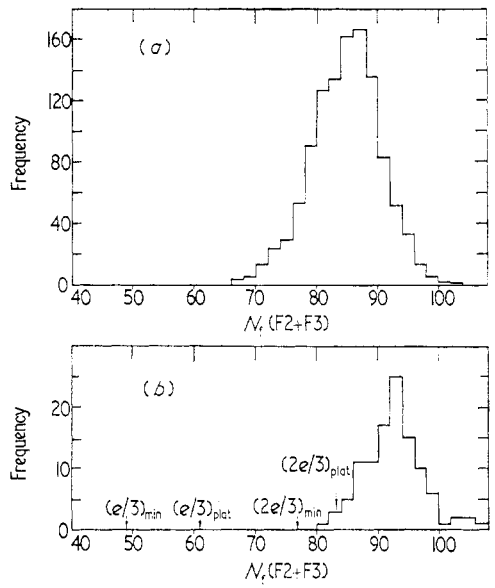

Figure 4. Frequency distributions of N_f, the number of flashes along the track in F2 + F3; run 1 data. Calibration was with single muon trigger. The expected positions of the quark peaks are indicated. The high voltage pulse was of exponential form (figure 2) and $T_D = 20\ \mu s$. (*a*) Calibration, 1131 tracks; mean = $84{\cdot}9 \pm 0{\cdot}2$, $\sigma = 5{\cdot}7$. (*b*) EAS, 111 tracks; mean = $91{\cdot}8 \pm 0{\cdot}4$, $\sigma = 4{\cdot}6$.

shower runs. Of immediate interest are two apparent quark candidates, having $N_f = 34$ and 43 in run 2 taken with EAS trigger; unfortunately, these events are attributable to edge effects, as will be discussed later, in § 8. An example of a selected shower, indicating accepted tracks, is given in plate 1.

As would have been expected, the tail of the run 1 data for calibration muons extends towards the $e/3$ quark region and the probability of spurious quarks is not completely negligible. With $T_D = 40\ \mu s$, however, the separation is considerable and it is to this set of data that detailed consideration will be given.

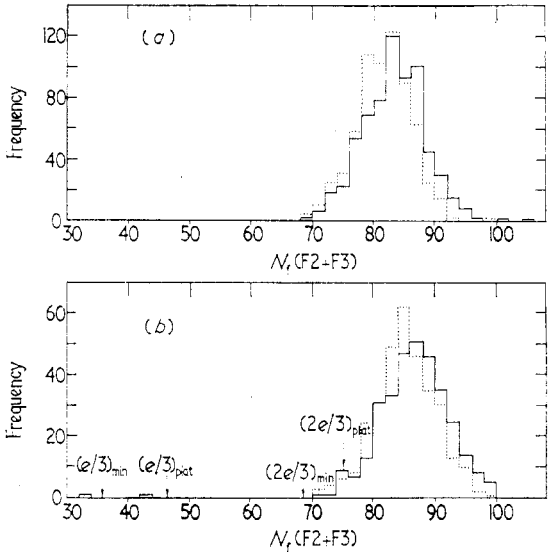

Figure 5. Frequency distributions of N_f, the number of flashes along the track in F2 + F3; run 2 and run 3 data. The high voltage pulse was of rectangular form (figure 2) and $T_D = 40\ \mu s$. The expected positions of the quark peaks correspond to the full line histogram. (*a*) Calibration, 666 tracks; full line, basic data; mean $= 82{\cdot}8 \pm 0{\cdot}2$, $\sigma = 5{\cdot}0$. Dotted line, corrected for angle; mean $= 81{\cdot}1 \pm 0{\cdot}2$, $\sigma = 4{\cdot}5$. (*b*) EAS, 328 tracks; full line, basic data; mean $= 86{\cdot}2 \pm 0{\cdot}3$, $\sigma = 5{\cdot}2$. Dotted line, corrected for angle; mean $= 84{\cdot}2 \pm 0{\cdot}3$, $\sigma = 4{\cdot}8$.

It should be pointed out at this stage that the muon calibration efficiency in run 1 is about 3% too low, a fact that is thought to be due to polarization effects in the glass of the flash tubes which resulted from a high muon repetition rate, of about $12\ min^{-1}$. For run 2 the muon calibration rate was less than one per minute and here the polarization effects are thought to be negligible. The polarization effect causes a tube which has flashed to be insensitive for some tens of seconds afterwards. Presumably a discharge causes a slowly decaying clearing field which sweeps out the electrons from a 'new' particle in the delay time T_D. The effect is eliminated in the EAS runs by imposing a dead time of 120 s after each event.

5. Sensitivity of response to particle ionization

As has been remarked already, the efficiency of the flash tube depends on the number of electrons produced by a particle in the neon gas, and since even for muons this quantity varies somewhat with momentum it will be momentum-dependent. An estimate of the variation has been found from run 2 and is shown in figure 6. The highest momentum point is taken from the observations on penetrating air shower particles. The three lowest momentum points are from data collected with calibration muons. In all cases the values of $\bar{N}_f$ from which the efficiency was found were multiplied by $\cos\theta$ so as to refer to $\theta = 0$. The subdivision into momentum bands

has been made on the basis of multiple scattering measurements in the chamber, appropriate corrections having been made for increased track lengths through scattering. A small correction has also been made to allow for extra flashes along the particle track in the EAS case, caused by accidental coincidence with the shower γ-ray induced flashes.

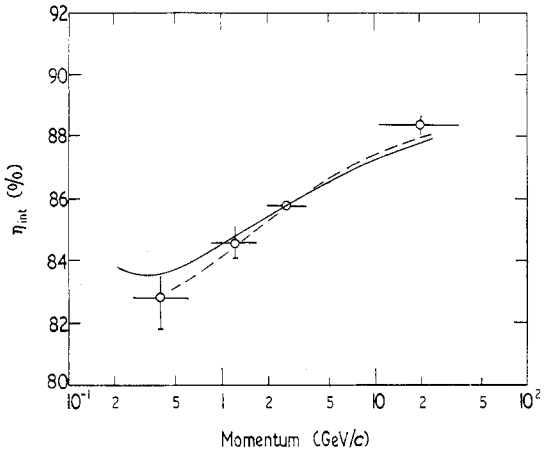

Figure 6. Variation of the mean internal efficiency, for F2 + F3, with momentum for the results of run 2. The full curve is derived from theory using the most probable ionization loss in neon as a function of momentum, and the broken curve includes a correction for unresolved knock-on electrons. Both are normalized to experiment at 2·1 GeV/c.

Comparison with theory has been made by taking the most probable energy loss in neon measured by Jones *et al.* (1963) together with the Lloyd theory with appropriate values of Q (§ 3). The result is the full curve in figure 6.

In fact, the comparison is not appropriate because of the distinction between average and most probable values; it is the average number of flashes which is recorded, whereas the theory relates to the most probable energy loss. To the latter must be added the effect of those close μ–e collisions in which a knock-on electron is generated which emerges at a small angle in the front plane, is not identified as such, and gives rise to extra flashes along the track. An approximate correction has been made for this effect with the result that, after normalization at the point at 2·1 GeV/c, the dotted line of figure 6 is to be adopted.

Comparison between the experimental points and the broken curve shows satisfactory agreement and, taken together with the arguments advanced in § 3, this leads us to believe that the correct response of the flash tube to ionization has been demonstrated.

6. Frequency distribution of number of flashed tubes

The method of derivation of the data given in figures 5 and 6 has already been explained, in § 4. At this stage it is necessary to examine the distributions in detail, to compare them with expectation and to predict, from the muon calibration data, the probability of observing pseudoquarks.

For a single layer of tubes and repeated traversal by independent particles Coxell and Wolfendale (1960) have given the following approximate expression for

the standard deviation of the layer efficiency:

$$\sigma_L = \eta_L(1-\eta_L)^{1/2}n^{-1/2}$$

where n is the observed number of flashes and η_L is the measured layer efficiency, that is, n divided by the number of traversals. The expression is valid if η_L is not too close to unity.

Turning to a stack of N_0 layers of tubes, application of this formula leads to a standard deviation in the number of flashes σ_f given by

$$\sigma_f = \{\eta_L(1-\eta_L)N_0\}^{1/2}.$$

This relation is not, of course, strictly applicable to the actual case of a regular stack of flash tubes because the underlying assumption of independent layers is not obeyed. However, it gives a rough indication of the expected standard deviation. The relation is shown graphically in figure 7.

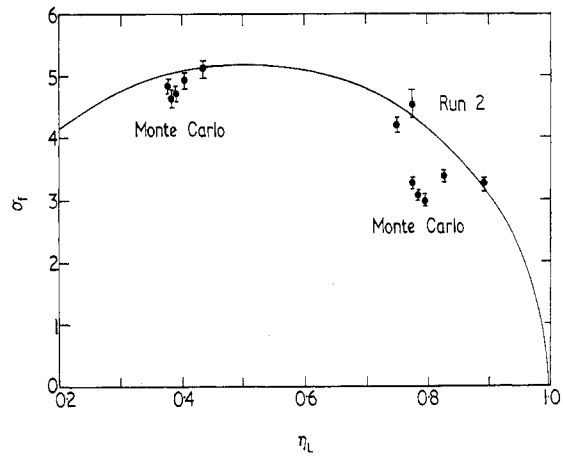

Figure 7. The standard deviation σ_f of the number of flashed tubes out of 108 layers (N_0) as a function of the mean layer efficiency η_L. The smooth curve represents $\sigma_f = \{\eta_L(1-\eta_L)\,N_0\}^{1/2}$ and corresponds to expectation for a random stacking arrangement. The results of Monte Carlo calculations are shown for two mean internal efficiencies, each set corresponds to five angles of incidence: 1 °, 7 °, 12 °, 20 ° and 29 °. The experimental points for calibration muons and EAS particles, have been corrected (a small reduction) for the distribution of both projected zenith and azimuthal angles so that they refer to vertical trajectories.

Also shown in this figure are the results of Monte Carlo calculations in which a computer analysis has been made of the numbers of tubes which would flash along trajectories of particles incident at a number of zenith angles (θ) and for two mean internal efficiencies 88·7% and 43·5%. The Monte Carlo data have not been standardized to the vertical direction and reading from left to right each set represents values of σ_f for θ = 1 °, 7 °, 12 °, 20 ° and 29 °. One thousand traversals were studied for each point and the error bars represent the statistical uncertainty.

Figure 7 also shows the value of σ_f calculated from the experimental data of figures 4 and 5. A small correction has been applied to allow for the uncertainty in azimuthal angle. It is seen that the experimental values are somewhat higher than

those from the Monte Carlo analysis. This feature is apparent in the actual distributions, shown in figure 8, and arises from a number of causes, notably unresolved knock-on electrons which cause a high N_f 'tail'.

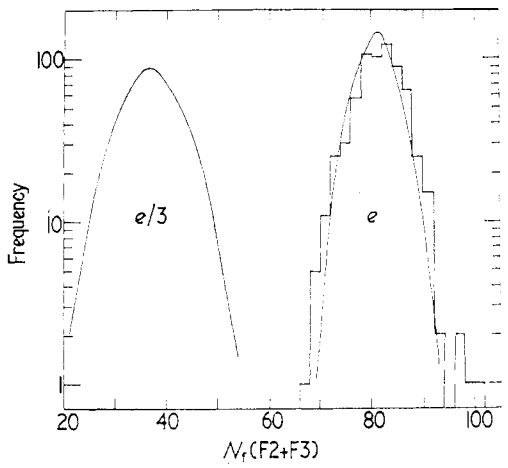

Figure 8. Frequency distribution of N_f(F2 + F3), run 2 data, for calibration muons. Also given are smooth curves drawn through the Monte Carlo results for e and $e/3$ particles. The latter have been broadened appropriately to allow for azimuthal obliquity.

In figure 8 the experimental values of N_f have been corrected for projected zenith angle (ie multiplied by cos θ) and the Monte Carlo distribution has been broadened to allow for the spread of azimuthal angles. The comparison is therefore precise.

Although the observed distribution is somewhat wider than expected, it is considered that it can be extrapolated to small values of N_f with sufficient precision to enable an estimate to be made of the probability of a muon simulating an $e/3$ quark. Using the data of figure 8, we estimated that an upper limit to the probability of a single muon having the necessary small number of flashes ($N_f < 55$) is 6×10^{-5} and that for less than 50 flashes is 8×10^{-6}. The rapid fall-off of probability with falling limit of N_f means that a limit can easily be chosen such that the probability of spurious quarks is sufficiently low and the loss of genuine quarks is small and calculable (for example, if we demand $N_f < 38$, half the genuine quarks are lost but the probability of a muon simulating a quark is much less than 10^{-6}).

7. Edge effects

In the Sydney experiment consideration was given to the presence of quarklike tracks due to field doubling where one half of the track was outside the illuminated volume because the ionized column was displaced by the electrostatic clearing field. It is interesting to note that there is an effect with flash tubes which bears some resemblance to it. This concerns muons which pass through the tubes outside the electrodes and cause a flash with reduced efficiency.

In the present experiment, for runs 1 and 2 the tubes are longer than the electrodes and the edge effect can be quite serious. Figure 9 shows the variation of efficiency

with distance from the edge of electrodes, the measurements being made with the aid of the azimuthal tubes. The extent of the transitional region is suprisingly large and some examination of its cause is necessary. Two factors contribute:

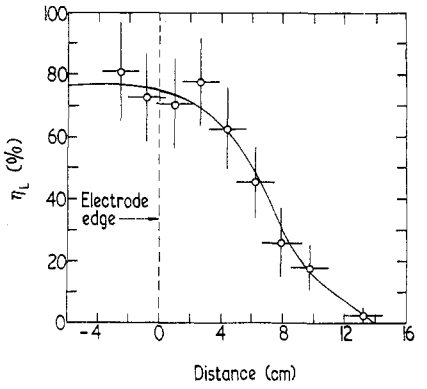

Figure 9. The variation of mean layer efficiency with distance from the electrode edge when tubes of length greater than the electrode length are used. The flashes beyond 4 cm are presumed to be due in the main to photons generated in weak discharges which then produce photoelectrons between the electrodes.

(i) the diffusion of electrons during the time delay T_D with a resultant finite probability of there being one or more in a region of high field which causes a flash.

(ii) The finite value of the electrostatic field away from the edge of the plates (see the Appendix) which can cause a flash with reduced efficiency.

The diffusion of electrons in a tube has been examined by Lloyd (1960). To a first approximation the problem can be treated as one dimensional so that the transitional region of efficiency would be expected to be of order $(2DT_D)^{1/2}$ where D is the diffusion coefficient. Substituting $D = 2280$ cm^2 s^{-1} for neon at 60 cm pressure (Lloyd 1960) gives 0·43 cm for $T_D = 40$ μs. Thus the diffusion effect will be small.

The fringing field is shown, in the Appendix, to fall rapidly with increasing distance from the plate edge, the mean field falling to 50% after 1·6 cm and 10% after 5 cm. Thus it appears that trajectories through very low fringing fields are able to generate a subsequent flash. This is not necessarily inconsistent with the data of figure 3, which shows the variation of internal efficiency (from photographed flashes) with field on the plates as a whole. Presumably the mechanism is that the very low fringing field causes a small discharge, too weak to be photographable, from which photons cause a complete discharge between the plates where the field is 'normal'.

As mentioned already (§ 4) two events were recorded in run 2 which contained tracks where N_f was low and which were classed as quark candidates. One of these is shown in plate 2. Unfortunately the azimuthal tubes were not working but some information about the azimuthal angle comes from the fact that the muon tracks are all seen from top to bottom of the chamber; this means that azimuthal angle is very small, ie the shower is nearly vertical in the side view. For a truly vertical shower the data of figure 9, together with the geometry of the chamber, indicate that as many as one in 25 muons will appear in the $e/3$ region (although, as will be seen later, they will be recognized as spurious).

For the two events in question, there is an overwhelming indication that these candidates are edge tracks. This comes from the observation that there is a large excess of pairs of adjacent flashes which bracket the high voltage electrodes. Such behaviour is not observed with tracks of comparable $\bar{N}_f$ derived from muons observed under conditions of much longer time delay and it is considered to be due to an edge effect where the inward directed field near this electrode brings discharges towards higher field regions. Thus, no genuine quark events remain in run 2 (although if there had been some they would have been recognized as such).

After the realization of the importance of edge effects the electrodes for F1 and F4 were shortened by 11 cm at each end (front and back) and a further period of observation was undertaken (run 3). For this set, too, it was demanded that tracks should be seen in F1 and F4 but now the selected particles must have passed well away from the edge and within the fully sensitive region of F2 and F3. No further low N_f events were seen in run 3.

It is concluded that no acceptable quark candidates remain.

8. Discussion

Although the number of selected EAS tracks accumulated so far is not large (439) it is of interest to compare the present upper limit to the quark flux with that reported by the Sydney group. In the present work the absorber cut out the bulk of the electron component so that, under the reasonable assumption that all quarks can penetrate this absorber, our result corresponds to no events amongst about 13 000 particles (the μ/e ratio is of the order of 3%). In the Sydney work the majority of the events were recorded in unshielded cloud chambers and 5 'quarks' appeared amongst about 60 000 tracks. However, the majority of the tracks did not satisfy the necessary stringent measurement criteria and, indeed, Cairns and Peak (1969) found that 3 of the 'quarks' appeared in 303 carefully selected tracks, that is 1 per 100 tracks. Our observation of none per 13000 particles would therefore appear to be inconsistent with the Sydney result.

Appendix. Fringing field at edge of flash-tube electrodes

The observation of low-efficiency events attributable to muons passing close to the edge of the electrode assembly has led to an examination of the magnitude and direction of the fringing field. The problem is a classic one in electrostatics and the elements of the solution have been given by Maxwell (1873). This author also gives a diagram showing equipotentials and lines of force rather close to the edge. In the present work the problem has been solved for a wider range of distances by the standard reiterative method for the solution of Laplace's equation (eg Shire 1960) using a computer; in this method (see figure 10) potentials are chosen at grid points such that $V_0 = \frac{1}{4}(V_1+V_2+V_3+V_4)$. The results for the magnitude of the resultant field in terms of E_0, the field well within the plates, are shown in figure 10 for various planes parallel to the plates. In the calculations the plane of symmetry has been taken as being at zero potential as has a perpendicular plane at a distance $4L$ from the edge of the plates. It has been assumed that the length and breadth of the plates are both very much greater than L.

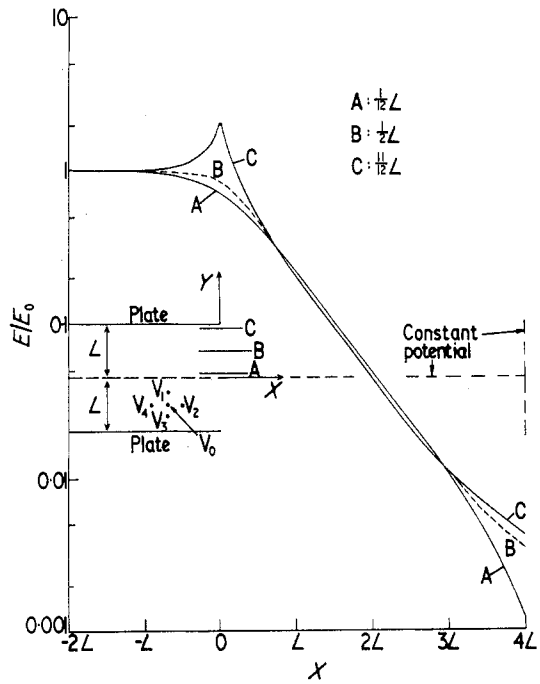

Figure 10. Fringing field near the edge of a set of parallel plates of large area. E is the magnitude of the resultant field for Y = constant at points along the X axis. A plane of constant potential is assumed to be situated at a distance equal to twice the plate separation. The electrode configuration shown in the inset is repeated above and below.

Acknowledgments

The authors are grateful to Professor G. D. Rochester and Dr G. H. Stafford for their support and to Drs J. M. Breare, M. G. Thompson and K. E. Turver for useful suggestions.

The Science Research Council are thanked for the provision of research grants and the Research Corporation are thanked for financial support to JK.

References

ADAIR, R. K., and KASHA, H., 1969, *Phys. Rev. Lett.*, **23,** 1355–8.
ASHTON, F., *et al.*, 1968, *J. Phys.* A: *Gen. Phys.*, **1,** 569–77.
ASHTON, F., EDWARDS, H. J., and KELLY, G. N., 1969, *Phys. Lett.*, **29B,** 249–51.
ASHTON, F., and KING, J., 1971, *J. Phys.* A: *Gen. Phys.*, **4,** L31–4.
CAIRNS, I., MCCUSKER, C. B. A., PEAK, L. S., and WOOLCOTT, R. L. S., 1969, *Phys. Rev.*, **186,** 1394–400.
CAIRNS, I., and PEAK, L., 1969, *Res. Report*, University of Sydney.
COXELL, H., and WOLFENDALE, A. W., 1960, *Proc. Phys. Soc.*, **75,** 378–86.
HAZEN, W. E., 1971, *Phys. Rev. Lett.*, in the press.
JESSE, W. P., and SADAUSKIS, J., 1955, *Phys. Rev.*, **97,** 1668–70.
JONES, D. G., WEST, R. M., and WOLFENDALE, A. W., 1963, *Proc. Phys. Soc.*, **81,** 1137–9.
KIRALY, P., and WOLFENDALE, A. W., 1970, *Phys. Lett.*, **31,** 410–2.
LLOYD, J. L., 1960, *Proc. Phys. Soc.*, **75,** 387–94.
MCCUSKER, C. B. A., and CAIRNS, I., 1969, *Phys. Rev. Lett.*, **23,** 658–9.
MAXWELL, J. C., 1873, *Treatise on Electricity and Magnetism*, Vol. 1, 3rd edn (London: Oxford University Press) p. 297.
SHIRE, E. S., 1960, *Classical Electricity and Magnetism* (London: Cambridge University Press), p. 35.
STERNHEIMER, R. M., 1956, *Phys. Rev.*, **103,** 511–5.

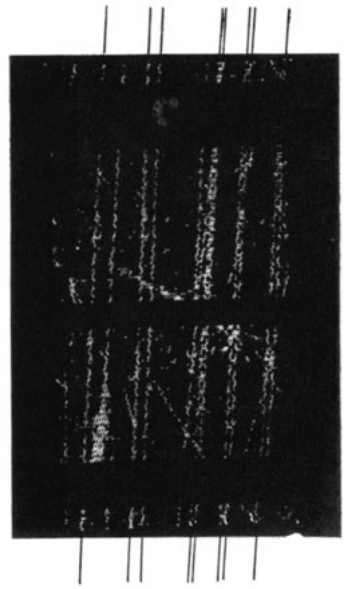

Plate 1. Example of a shower. The tracks accepted for measurement are indicated.

Plate 2. A shower showing a 'quark candidate'. The broken line indicates the candidate.